Preorogenic exhumation of the North Pyrenean Agly massif (Eastern Pyrenees-France)

Alain Vauchez, Camille Clerc, Lucie Bestani, Yves Lagabrielle, Alain Chauvet, Abdeltif Lahfid, David Mainprice

TECTONICS, VOL. 32, 95–106, doi:10.1002/tect.20015, 2013

Preorogenic exhumation of the North Pyrenean Agly massif (Eastern Pyrenees-France)

Alain Vauchez,[1] Camille Clerc,[1,2] Lucie Bestani,[1,4] Yves Lagabrielle,[1] Alain Chauvet,[1] Abdeltif Lahfid,[3] and David Mainprice[1]

Received 18 June 2012; revised 16 December 2012; accepted 8 January 2013; published 1 March 2013.

[1] The Pyrenees, north of the North Pyrenean fault, display a complex structure involving a succession of peridotite massifs, basement massifs, and mid-Cretaceous to Late Cretaceous basins located in a narrow domain, which was affected by a mid-Cretaceous, preorogenic, high-temperature, low-pressure metamorphism. The Late Cretaceous basins were interpreted either as pull-apart basins formed during transcurrent motion of Iberia relative to Eurasia or as remnants of a larger extensional basin. Recent models support that peridotite massifs result from the exhumation of the mantle during this preorogenic event. The northern boundary of the Agly basement massif shows evidence of ductile deformation of the basal formations of the Agly sedimentary cover. Macroscopic and microscopic kinematics indicators consistent with asymmetry of crystallographic fabrics suggest normal sense of shear and thus suggest detachment, at least partial, of the Mesozoic cover from its basement. Triassic to Early Cretaceous limestones are mylonitic and consistently shows a foliation, a NS- to NE-trending lineation, shear criteria suggesting top-to-the-north shearing and locally boudinage. At the microscopic scale, mylonites are characterized by a very fine grain size, frequently <10 μm. They contain larger, partially recrystallized calcite parent grains and undeformed quartz grains with calcite fringes crystallized in pressure shadows. In these mylonites, calcite systematically shows a weak but well-defined crystallographic-preferred orientations, suggesting HT dislocation creep combined to diffusion creep and possibly grain boundary sliding in the finest fraction of the mylonites. Paleotemperatures determined using Raman spectrometry suggest synkinematic temperature conditions in the range 340–390°C, in good agreement with observed microstructures and calcite CPO. The mylonitic fabric in Mesozoic limestones is folded by EW-trending Pyrenean folds north of the Agly basement massif, attesting that this fabric formed before the Pyrenean orogeny. These data consistently support preorogenic extension under medium-temperature conditions of the northern Agly massif and likely of the massif itself. Since simultaneously (~100 Ma) a mid-Cretaceous basin opened south of the basement massif, we suggest a model of preorogenic exhumation of the Agly massif in response to the regional extension associated to the rotation of Iberia. This model may explain the exhumation of the North Pyrenean massifs during a single preorogenic event that allowed the opening of extensional basins and the exhumation of the lithospheric mantle. All these structures being subsequently reworked during the Pyrenean orogeny.

Citation: Vauchez, A., C. Clerc, L. Bestani, Y. Lagabrielle, A. Chauvet, A. Lahfid, and D. Mainprice (2013), Preorogenic exhumation of the North Pyrenean Agly massif (Eastern Pyrenees-France), *Tectonics*, *32*, 95–106, doi:10.1002/tect.20015.

[1]Geosciences Montpellier, CNRS UMR-5243, Université de Montpellier II, Montpellier, France.
[2]Laboratoire de Géologie, CNRS UMR-8538, Ecole Normale Supérieure, Paris Cedex 5, France.
[3]BRGM/LMA /MIN, Orléans, France.
[4]CEREGE, Technopôle de l'Arbois-Méditerranée, Aix en Provence cedex 4, France.

Corresponding author: Alain Vauchez, Geosciences Montpellier, CNRS UMR-5243, Université de Montpellier II, Place E. Bataillon, 34095 Montpellier, France. (alain.vauchez@um2.fr)

0278-7407/13/10.1002/tect.20015

1. Introduction

[2] The Pyrenean belt is divided in two main domains by the ~EW-trending North Pyrenean Fault (NPF) that underlines the corridor along which the Late Cretaceous rotation of the Iberian microplate relative to the Eurasian plate was accommodated [*Larrasoaña et al*., 2003; *Le Pichon et al*., 1970; *Srivastava et al*., 1990]. The Pyrenean belt north of the NPF displays peculiar features that mainly result from its preorogenic history. These features, present along the entire belt from East to West (Figure 1), include discontinuous hercynian basement massifs (the "North Pyrenean massifs"), numerous bodies

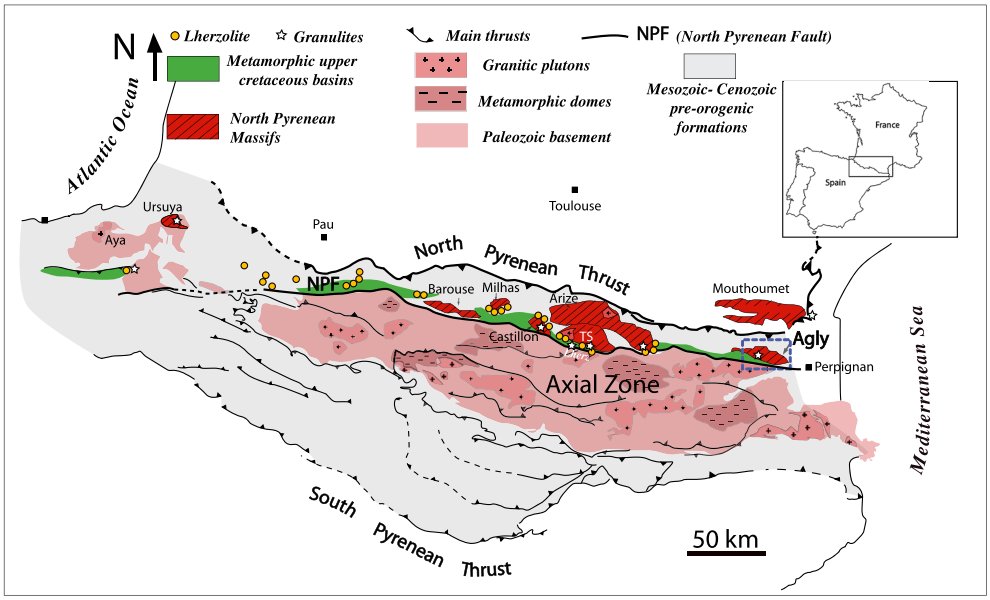

Figure 1. Simplified map of the Pyrenees showing the location of the north Pyrenean basement massifs, the orogenic peridotites massifs, and the late cretaceous metamorphic basins. The original geometry of these massifs as well as their relations with the North Pyrenean transform zone (now reduced to the North Pyrenean Fault, NPF) have been deeply modified by the Pyrenean orogeny. TS is for Trois Seigneurs basement massif. Location of 1) peridotites and granulite massifs after Lagabrielle and Bodinier 2008 and 2) Upper Cretaceous, metamorphic basins after *Choukroune* [1992].

of subcontinental peridotites of various sizes, and mid-Cretaceous to Late Cretaceous inverted metamorphic basins.

[3] The inverted metamorphic basins have been interpreted as a succession of pull-apart basins formed during the transcurrent to transtensional movement of the Iberian microplate along the NPF during the opening of the Bay of Biscay [*Choukroune and Mattauer*, 1978]. However, more recent works suggest the formation of a larger extensional domain between Iberia and Eurasia in association with the transcurrent motion [*Sibuet et al*., 2004; *Stampfli and Hochard*, 2009]. The lithospheric thinning that occurred in those basins due to the Iberian microplate displacement relative to Eurasia also triggered an HT metamorphism (105–90 Ma) that affected the sediments deposited in the basins. This HT metamorphism indeed extend northward in a domain that encompasses Mesozoic sediments, the basement massifs, and the mantle peridotites [*Goldberg and Leyreloup*, 1990; *Clerc et al*., 2012]. Tectonic inversion of the preorogenic basins occurred during the Eocene-Oligocene Pyrenean compression [e.g., *Choukroune*, 1992].

[4] Processes accounting for the exhumation of mantle peridotite and basement massifs as well as the timing of this exhumation (pre- or syn-orogenic) are still questioned. Recently, *Lagabrielle and Bodinier* [2008] and *Lagabrielle et al*. [2010] have reported evidence supporting that the Lherz peridotite massif was exhumed in relation with Aptian-Albian extreme crustal thinning associated to the motion of Iberia relative to Europa, i.e., coeval with the mid-Cretaceous opening of the basins and the preorogenic "Pyrenean" metamorphism. This model, also defended by *Jammes et al*. [2010], is in good agreement with the suggestion that normal faulting and ductile shearing dated at 110–100 Ma affect the hercynian crystalline massifs in the Pyrenees [*Passchier*, 1984; *Costa and Maluski*, 1988; *Saint Blanquat*, 1990; *Paquet and Mansy*, 1991]. In addition, crustal thinning is shown to have been coeval with a thermal event that affected the Pyrenean continental basement. Active circulation of hot fluids led to overall albitization in the Agly, Salvezine, Saint Barthelemy, and Arize North Pyrenean massifs, where the fluid circulation is dated between 117 and 98 Ma [*Poujol et al*., 2010]. Moreover, in the Saint Barthélémy massif, the formation of the Trimouns talc at the expense of dolomitic Paleozoic formation lasted at least 10–15 Ma during the Albian [*Schärer et al*., 1999]. The talc is strongly deformed within a shear zone that cuts the whole massif. This implies that a major deformation event affected the basement block during the mid-Cretaceous [*Passchier*, 1984; *St. Blanquat et al*., 1986; *St. Blanquat*, 1993]. This gently dipping shear zone shows a top-to-south kinematics and is associated with an important thinning of the crust in an extensional context [*Passchier*, 1984; *St. Blanquat et al*., 1986]. These features collectively suggest that the north Pyrenean basement massifs have been thinned and uplifted in response to the processes accounting for the exhumation of the subcontinental mantle during the Aptian-Albian.

[5] In this article, we report new data on the deformation and paleotemperatures of the northern part of the Agly massif, the easternmost north Pyrenean massif, that substantiate medium-temperature extensional shearing and mylonitization of the Mesozoic cover along the contact with basement rocks. This extensional deformation clearly predates the Pyrenean orogeny; it was coeval with the preorogenic metamorphism and the opening of the Late Cretaceous Boucheville basin. These data point to a preorogenic exhumation of the Agly hercynian massif in

response to a regional-scale extension triggered by the rotation of the Iberian microplate.

2. Geological Setting

[6] The Agly massif (Figure 2), the easternmost hercynian massif of the northern Pyrenees, is bounded to the south by the Boucheville syncline, one of the Cretaceous metamorphic basin inverted during the Pyrenean orogeny, and to the north by the Agly overturned syncline that involves the Mesozoic cover. The boundary between the Boucheville syncline and the basement is marked by a major subvertical fault that put in contact variscan granulites and charnockites with Aptian-Albian flysch. This extensional fault, formed in relation with the basin opening, has been subsequently reactivated and displays evidence of postmetamorphic transcurrent and more locally reverse movements.

[7] The Agly basement massif is divided in two parts: the northeastern domain consists of northeastward to eastward gently dipping lower Ordovician metapelites affected by a low pressure metamorphism that increases downward from greenschists facies conditions (~350°C, <200 MPa) to upper amphibolite facies conditions (600–650°C, <400 MPa). The southwestern domain consists of high-grade gneisses (up to granulite facies) and magmatic intrusives [*Vielzeuf and Kornprobst*, 1984]. The highest-grade rocks are anatectic granulites and charnockites. They occur close to the southern contact with the Boucheville Cretaceous basin. The contact between the two basement domains (Figure 2) was interpreted as a normal fault, gently dipping to northeast, related to late variscan extension [*Bouhallier et al.*, 1991]. Indeed, the variscan basement displays many north- to northeast-dipping extensional shear zones. These shear zones formed under relatively low-temperature conditions: strain is strongly localized in centimeter- to meter-wide mylonitic to ultramylonitic zones. Many of these shear zones display evidence of deformation at the ductile-brittle transition. K-feldspars undergone microfracturation ("granulation") leading to cataclastic flow and quartz deformed through low-T crystal plasticity marked by incipient dynamic recrystallization in strongly elongated grains (Figure 3).

[8] In the northeastern part of the massif, the "Pyrenean" (Eocene-Oligocene) orogenic imprint is limited. The Mesozoic sediments that border the basement are concordant with the schistosity of the Silurian and Devonian metapelites. The western part is affected by several "Pyrenean" thrust faults that make it more difficult to evaluate the preorogenic relationships between the basement and its Mesozoic cover. The Mesozoic series (Triassic to Upper Cretaceous) mostly consists of limestones, some of which contain up to 10–15% of quartz and bioclasts, and subordinate shales. The Triassic formations, characterized by interbedded evaporites and quartz-

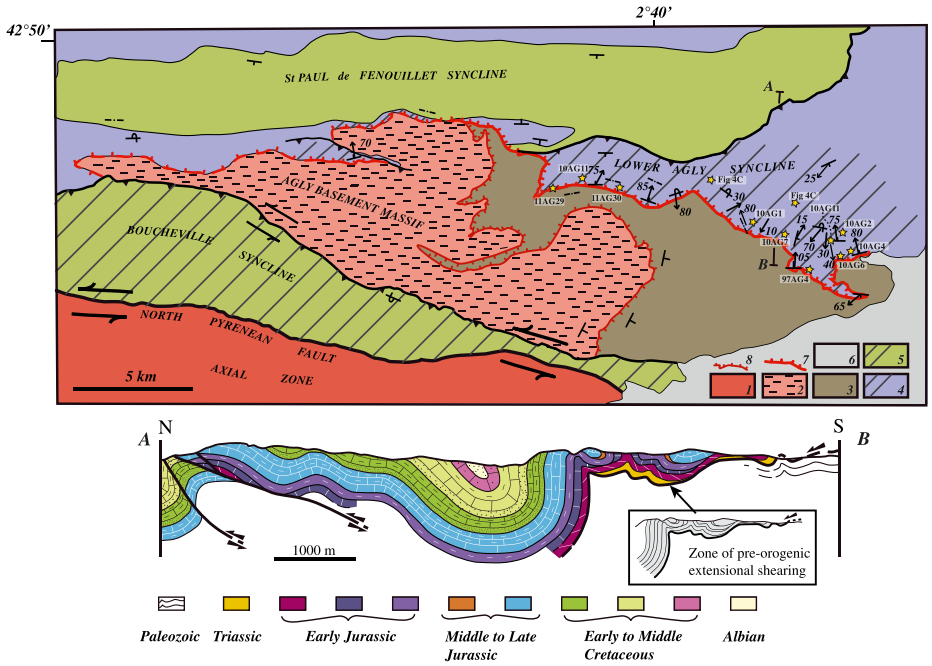

Figure 2. Schematic map and cross section of the Agly basement massif and its surroundings. *Map*: 1 = Variscan terranes of the axial zone; 2 = Amphibolite to granulite facies gneisses forming the deeper part of the Agly massif; 3 = Ordovician (amphibolite facies) to Devonian (greenschist facies) metasediments; 4 = Triassic to Early Cretaceous formations, stippled where affected by the preorogenic metamorphism; 5 = Late Cretaceous sediments, stippled where affected by the preorogenic metamorphism; 6 = postorogenic deposits; 7 = extensional contact between the Agly basement and its Mesozoic cover; 8 = extensional contact [*Bouhallier et al.*, 1991] between the lower part of the Agly basement and the Palaeozoic metasediments. Both extensional contacts have been reworked during the Pyrenean orogeny. Stars with numbers show the location of the samples used for CPO measurements and for most microphotographs. AB: cross-section showing the simplified structure of the northern boundary between the basement and its Mesozoic cover. Location of the cross section: AB on the map.

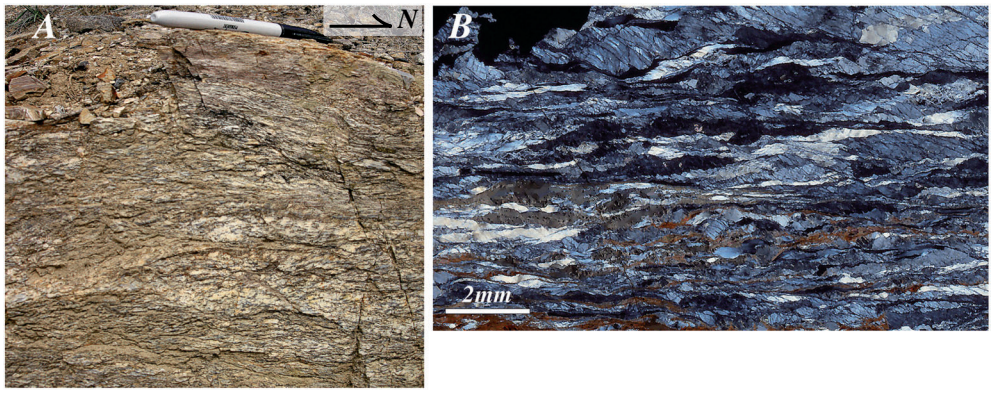

Figure 3. Low-temperature mylonitization of a variscan granite in an extensional shear zone. (a) A heterogeneous deformation of the granite in which mildly deformed domains alternate with zones of mylonites and ultramylonites. (b) An example of the microstructure in the mildly deformed granite. Quartz crystals are strongly elongated and display local dynamic recrystallization in ultrafine grains (a few micrometers); K-feldspars have undergone a cataclastic deformation. Thin section parallel to the *XZ* structural plane.

rich limestones, are discontinuous, boudinaged, and, consequently, frequently lacking.

3. Deformation of Mesozoic Rocks Close to the Basal Contact

[9] As already observed by *Legier et al.* [1987], the Triassic and Jurassic rocks above the northern boundary of the Variscan basement (Figure 2) display structures and microstructures typical of a ductile deformation. This deformation is stronger close to the contact with the basement and decreases upward in the Mesozoic series.

[10] Most rocks are fine-grained and display a conspicuous mineral lineation trending NS to NE-SW, more visible in impure than in pure limestones (Figures 4a and 5). Locally scapolite (dipyre) crystals are oriented parallel to the lineation. This stretching mineral lineation is folded by the Agly syncline and smaller satellite folds that affect the base of the Mesozoic series, especially along the better preserved northeastern boundary (Figure 2). In most cases, this lineation is associated with a foliation parallel to the stratification. In places where the foliation is oblique to the sedimentary bedding, geometrical relationships are not consistent with those expected for an axial-plane foliation related to the "Pyrenean" folds.

[11] Numerous evidence of syn-metamorphic stretching can be observed. Limestone layers are locally boudinaged at the outcrop scale (Figure 5). In 3D they display a "chocolate tablet" with a main elongation ~NS in agreement with the presence in the limestone of a strong, NNE-trending mineral stretching lineation (Figure 5b). At a larger scale, such boudinage resulted in lateral discontinuity of the Triassic and Lower Jurassic layers.

[12] At smaller scale, fossils are elongated and sometimes truncated and rotated in the direction of extension (Figure 4b). Although most limestones are very fine-grained, some macroscopic shear sense indicators have been observed that consistently suggest a top-to-north kinematics. For instance, macroscopic asymmetric fringes developed in pressure shadows around heterogeneities embedded in impure limestone (Figure 6). Overturned folds wrapped by the foliation (intrafolial folds) trend either EW or NS. In all cases, the hinges of these folds display an axial plane foliation that bears the mineral stretching lineation. Eocene-Oligocene compressional folds were superimposed to these early folds resulting in complex geometry [*Legier et al.*, 1987].

[13] At the thin section scale, limestones systematically display a mylonitic fabric characterized by a partial to complete dynamic recrystallization. The new grain size varies from <10 to ~40 μm, sometimes at the hand sample scale (Figure 7). In most cases, new grains are slightly elongated (up to 3:1) within the foliation even for grain size <10 μm. Frequently, remnants of parent calcite grains are observed (Figure 8). They display evidence of dislocation creep, such as undulose extinction and subgrains. Porphyroclasts display irregular shapes due to the presence of recrystallized new grains along their boundaries. Recrystallization preferentially occurred along the grain boundaries and in narrow zones that crosscut parent grains. Some porphyroclasts are strongly elongated within the foliation (Figure 9). In impure limestones, quartz remains almost undeformed due to its higher stiffness and display pressure shadows. In most cases, pressure shadows are symmetric or display a faint asymmetry; however, in some cases they are asymmetric and suggest a top-to-north sense of shear. In several samples, sigmoidal strain fringes filled with calcite fibers mark the pressure shadows (Figure 10), suggesting that fluids were present during deformation.

4. Crystallographic Preferred Orientation

4.1. Methodology

[14] Oriented samples of mylonitic limestones showing a clear lineation have been selected for crystallographic-preferred orientation (CPO) measurements. Calcite CPO was measured on carefully polished thin sections using the electron backscattering diffraction (EBSD) technique. Measurements were performed in automatic mapping mode on a grid basis of 2–15 μm in either a CamScan CrystalProbe X500FE or a JEOL JSM-5600 scanning electron microscope at Geosciences Montpellier (Université de Montpellier 2). In both cases, the sample is tilted at an angle of 70° relative to the electron beam, producing Kikuchi bands on a phosphorous screen. Diffraction images were recorded by a high-speed camera, then amplified and processed using the Channel 5 software (Oxford Instruments). Each measurement allows determining the nature of

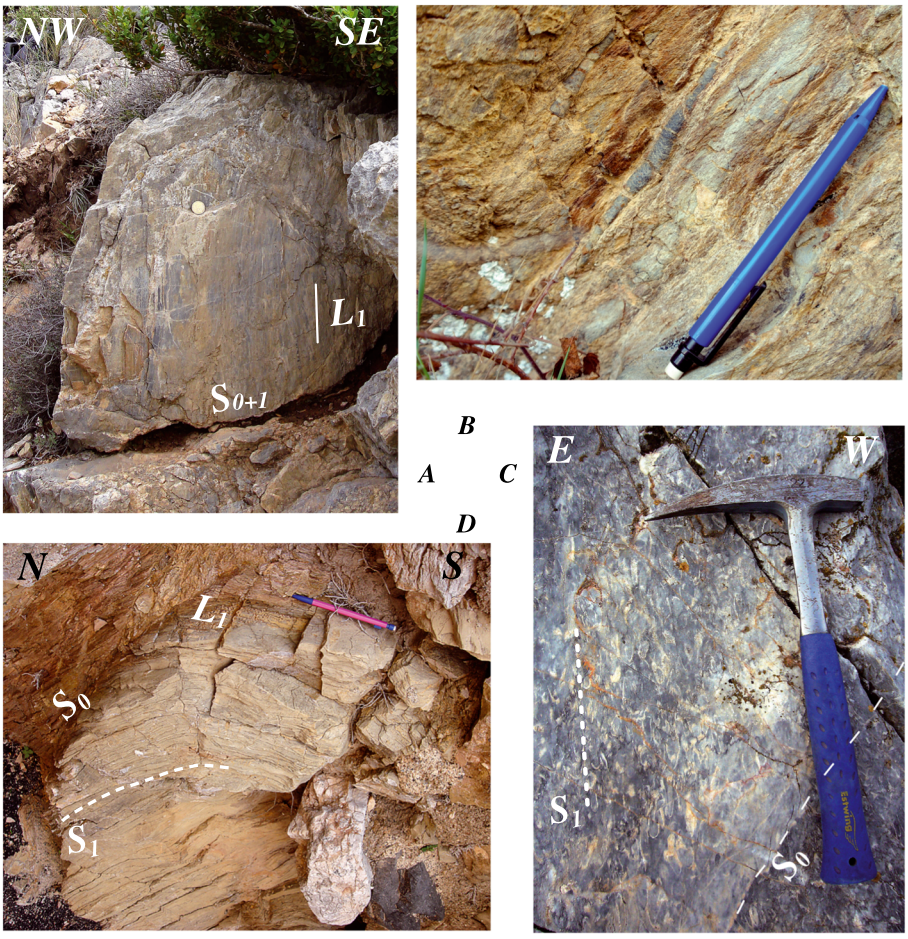

Figure 4. Tectonic fabric associated with the preorogenic ductile deformation of mesozoic metasediments. (a) The vertical southern limb of the Agly syncline shows a downdip stretching lineation almost orthogonal to the fold axis in early Jurassic limestones (10AG11). (b) A belemnite elongated ~NS, parallel to the stretching lineation in Early Jurassic limestones (10AG2). (c) The foliation (S_1) marked by stretched fossils, which cross-cuts the stratification in Late Jurassic limestones in the southern limb of the Agly syncline. (d) An isoclinal fold roughly coeval to ductile shearing in Early Jurassic limestones.

the mineral and the orientation of the crystal. Postprocessing of measurements include data filtering and averaging measurements for each crystal under the Channel 5 software. Pole figures (PF) were computed using the MTEX software [*Hielscher and Schaeben*, 2008; *Bachmann et al*., 2010; *Mainprice et al*., 2011]. In a PF, specific crystallographic axes or directions are plotted in the *XYZ* structural frame. All PFs have been processed using one single measurement per grain to give a similar weight to all grains independently of their size. Plotting one point per grain usually allows a better determination of the slip systems, especially when the grain size is bimodal. However, as shown in the next section, the grain size

Figure 5. (a) Boudinage of the Early Jurassic limestones. (b) The surface of a limestone layer located at the tip of a boudin, which bears a well-developed stretching lineation enhanced by weathering (10AG7).

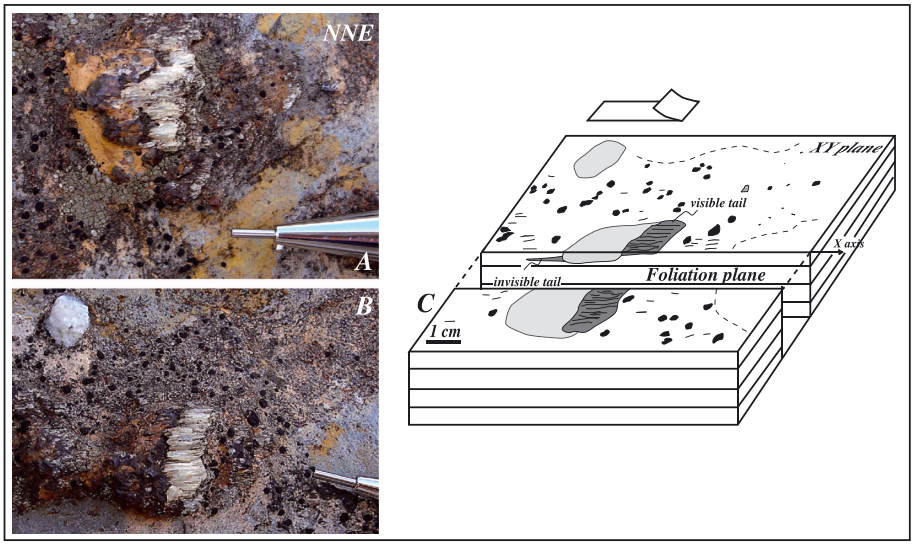

Figure 6. Calcite fringes crystallized in the pressure shadows around detritic bodies in Middle Jurassic limestones (a and b; close to sample 10AG2). Fringes are asymmetrically crystallized on both sides of stiff object, but only the upper (northern) tail is visible because the southern tail is still below the erosion surface, as seen on the interpretative cartoon (c).

can be an important factor that influences deformation mechanisms. For some samples, we thus plotted separately the CPO of calcite as a function of the grain size.

4.2. Calcite

[15] All studied samples display a weak but well-organized CPO. Different patterns have been obtained. For simplicity sake, implications of each CPO type are provided after each observation, and then a general discussion is provided in the "*Discussion and Conclusions*" section.

- Several samples, with a mean recrystallized grain size of a few tenths of micrometers, display a point concentration of ***c***[0001] close to the pole to the foliation with a slight asymmetry and a concentration of $\boldsymbol{a}<2\bar{1}\bar{1}0>$ in a direction close to the lineation (Figure 11). This pattern suggests that the deformation was accommodated by dominant slip on the ***c***(0001) plane with $\boldsymbol{a}<2\bar{1}\bar{1}0>$ as slip direction [e.g., *Pieri et al.*, 2001].
- In a few cases, $\boldsymbol{e}<\bar{1}012>$ is closer to the pole of the foliation and ***c***[0001] define a point concentration on one side of the pole figure. Because $(\bar{1}012)$ is not known as a slip plane and there is very few evidence of twinning, even in porphyroclasts, this asymmetric pattern is likely due to a simple shear deformation with (0001) as dominant slip plane.
- Several very fine-grained (≤10 μm) calcite mylonites, some embedding coarser, partially recrystallized grains, display a point maximum concentration of *c* axes close to the lineation or at an angle of ~30° (Figure 11). The fabric strength is always low, but the concentration of *c* axes is well defined.

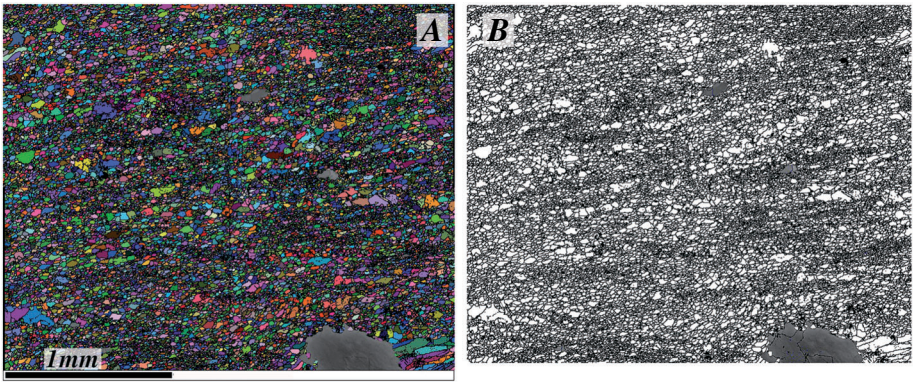

Figure 7. Electron back-scattering diffraction (EBSD) map showing the typical microstructure in a totally recrystallized domain of a mylonitic limestone (sample 10AG6). Colors in Figure 7a are a function of the crystallographic orientation of calcite (quartz grains are grey), and Figure 7b shows an automatic grain boundaries drawing derived from Figure 7a. In this sample, the grain size is variable, with domains containing very fine grains (~10 μm) alternating with domain in which the recrystallized grain size is larger (30–50 μm). The repartition of grain size domains marks the flow fabric. A large proportion of grains, independent of the grain size, display an elongate shape. Thin section parallel to the XZ structural plane.

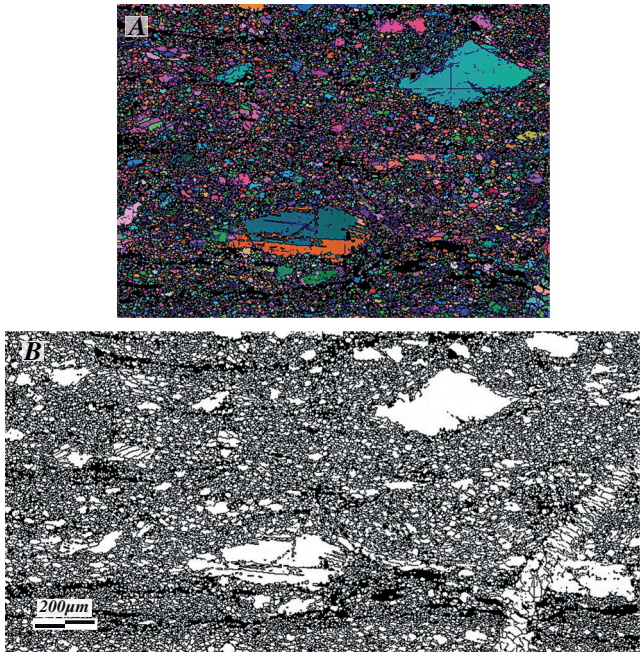

Figure 8. EBSD map of a sample (10AG20B) containing large remnants of calcite parent grains in a finely recrystallized matrix. (A and B) as in Figure 7. Porphyroclasts show elongate shapes, contorted grain boundaries, and evidence of dynamic recrystallization. Thin section parallel to the *XZ* structural plane.

This crystallographic fabric is puzzling since it suggests ***c***[0001] as slip direction, but this axis has never been determined as an active slip direction in experimental deformation of calcite aggregates.

[16] To investigate in more detail this unexpected CPO, we have divided the population of calcite crystals of the aggregates in several groups depending on their grain size (Figure 12). In several samples, the orientation of ***c***[0001] parallel to the lineation is clear for crystals with a small grain size, although the fabric strength decreases for the smallest one. In contrast, this orientation is not found for the coarsest grains that display a concentration of ***c***[0001] close to the pole to the foliation (Figure 12). This suggests a change in deformation mechanism associated with grain size reduction due to dynamic recrystallization. Such variation of the CPO with the grain size is however not systematic. Sample 97AG4b (Figure 11), for instance, displays a concentration of ***c***[0001] close to the *X* axis, independent of the grain size. It should, however, be noticed that this sample contains almost no remnants of original grains and that the variation in grain size is among recrystallized crystals.

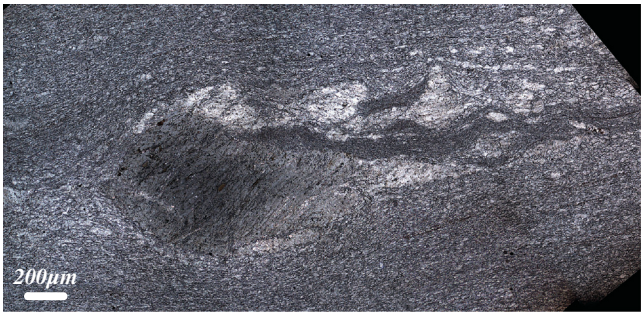

Figure 9. "Retort-shaped" calcite crystal embedded in a finely recrystallized calcite matrix (~80% have a grain size <15 µm and ~50% <10 µm). The mylonitic foliation wraps around the porphyroclasts, the upper part of which was more strongly sheared than the lower part and displays evidence of dynamic recrystallization. Polarized-analyzed reflected light. Sample 10AG1B. Thin section parallel to the *XZ* structural plane.

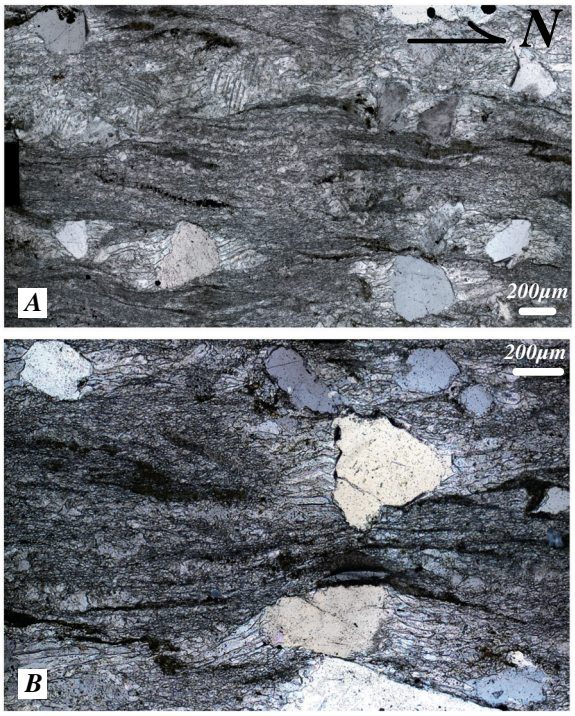

Figure 10. Asymmetric calcite fringes around quartz crystals. Black strips along the foliation are organic matter. Polarized-analyzed reflected light. Sample 10AG6. Thin section parallel to the *XZ* structural plane.

4.3. Quartz

[17] Quartz does not display any reliable preferred orientation even in samples that are relatively quartz-rich. This observation is not surprising since quartz is less ductile than calcite and behaves as rigid objects in the calcite matrix, especially under temperature conditions close to its brittle-ductile transition. This behavior is well illustrated by the development of fringes in pressure shadows around quartz grains.

5. Paleotemperatures From Raman Spectroscopy

[18] The Raman spectroscopy has been used successfully to characterize the structural evolution of carbonaceous materials (CM), reflecting a transformation from disordered CM to well-ordered CM [*Wopenka and Pasteris*, 1993], during metamorphism. The irreversible polymerization and reorganization of these materials allow estimating peak temperatures of metamorphic rocks using the Raman CM geothermometer with the R2 Raman

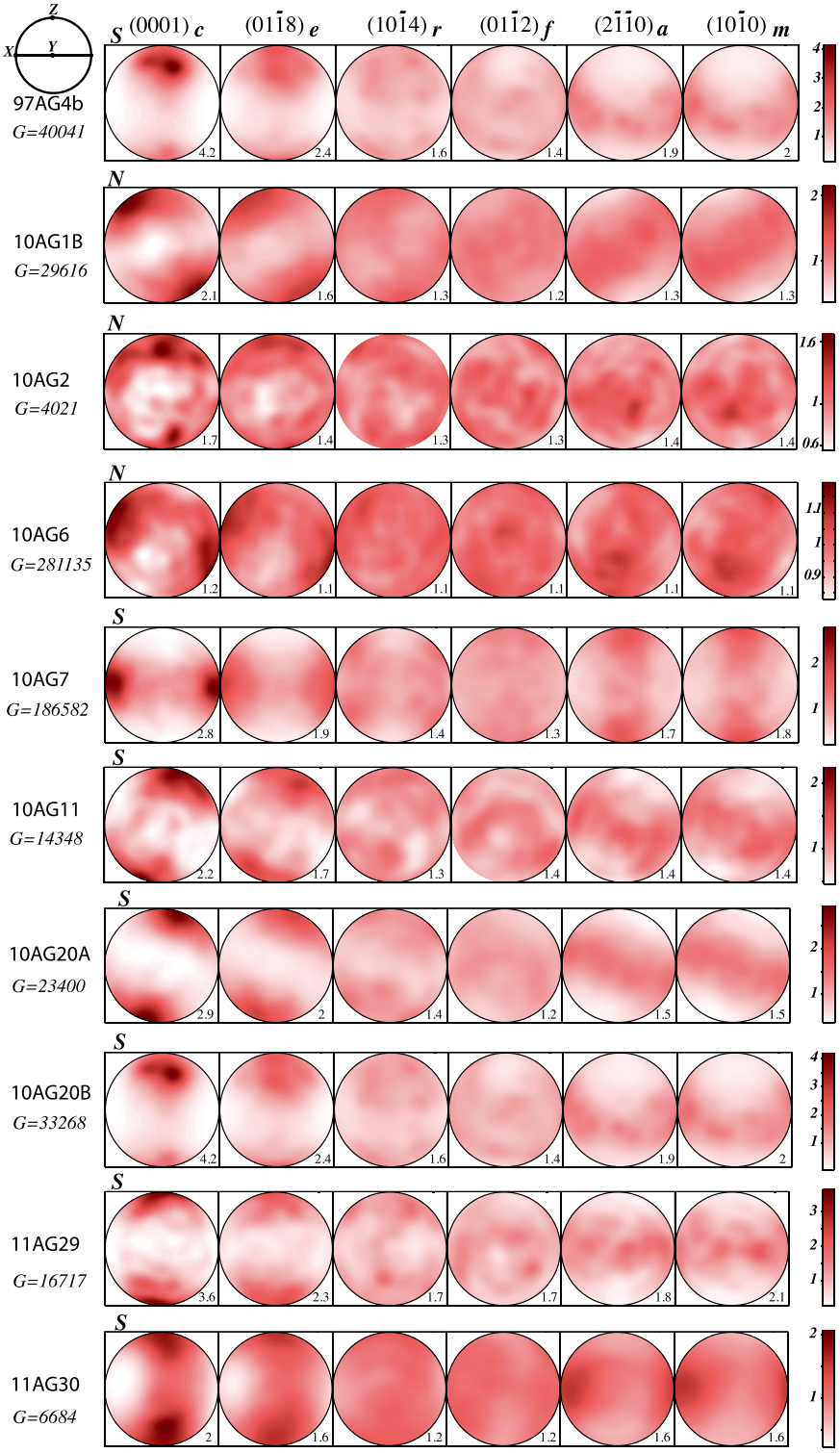

Figure 11. Crystallographic preferred orientation (CPO) of calcite in mylonitic limestones close to the contact with the hercynian basement (see location of samples on Figure 2). All samples display a well-defined although weak CPO. Samples 10AG1B, 10AG2, 10AG 11, 10AG20A and B, 11AG29 and 11AG30 show a concentration of (0001)*c* at a small angle to the pole of the foliation suggesting the basal plane as main slip plane and $(2\bar{1}\bar{1}0)a$ as main slip direction. Several other samples: 10AG6, 10AG7, 97AG4b display concentrations of (0001)*c* close to the lineation and $(2\bar{1}\bar{1}0)a$ close to the pole to the foliation. This latter CPO would suggest (0001)*c* as slip direction, a system that has never been suggested by experimental work. See further discussion in the main text. G is the number of grains that have been measured. N is North. XYZ on diagram in the upper left corner are the main axis of the strain ellipsoid, X = lineation, Z = pole to the foliation, Y = intermediate axes orthogonal to the lineation in the foliation plane.

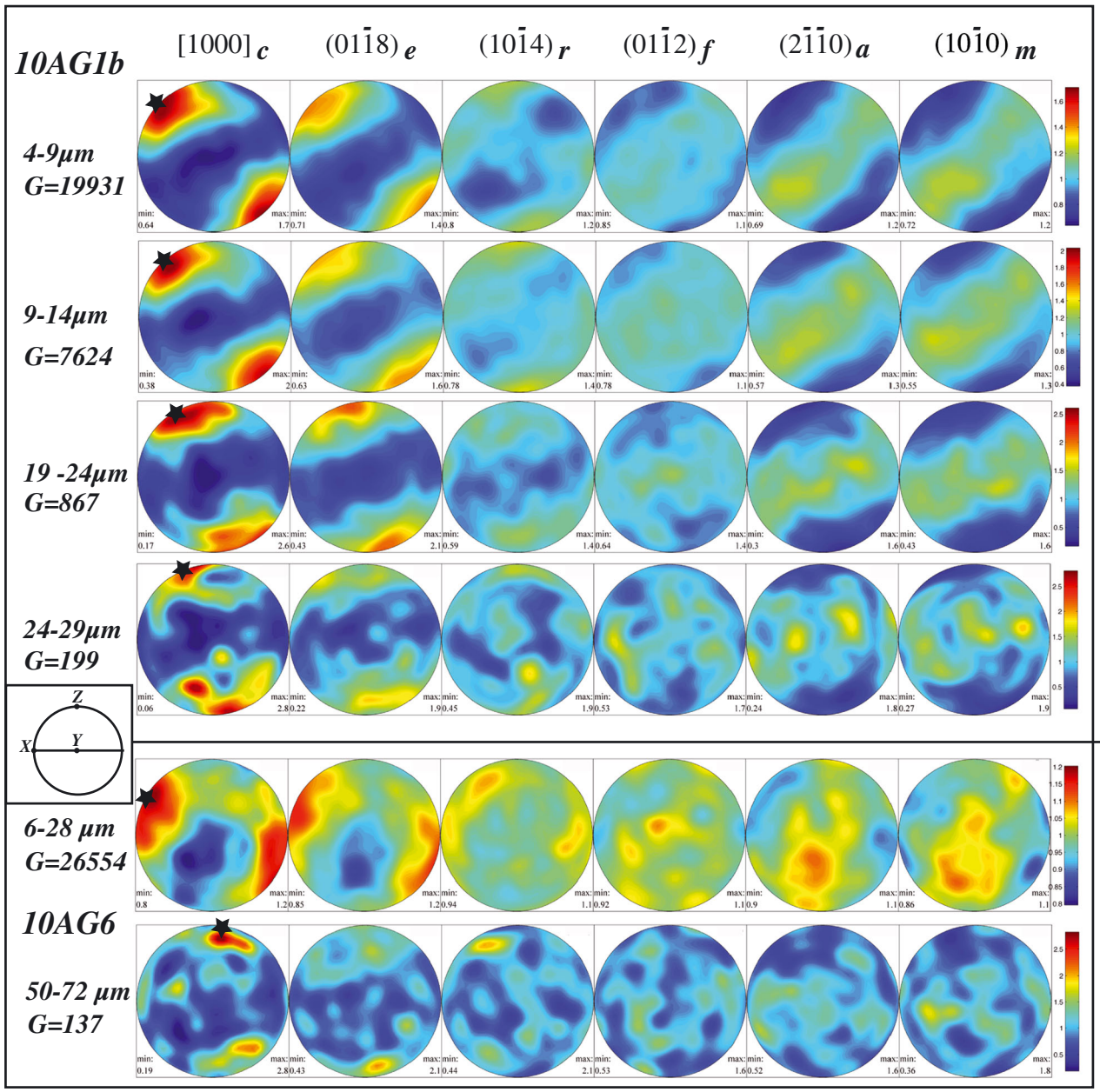

Figure 12. Pole figures showing the variation of calcite CPO with the grain size in two samples having retained calcite porphyroclasts. In both samples, fractions with larger grain size (with enough grains to be statistically reliable) are characterized by a maximum of [0001] close to the pole to the foliation (*Z* axes), while fractions with the finest grain size display a concentration of [0001] either between the *X* and *Z* axes or closer to the *X* axes. Grain size and grain size classes (30–50 bins) were automatically determined from EBSD measurement using the MTEX software [*Hielscher and Schaeben*, 2008; *Bachmann et al*., 2010; *Mainprice et al*., 2011].

parameter [*Beyssac et al*., 2002]. In this study, we have applied the Raman geothermometric approach of *Beyssac et al*. [2002] to estimate paleotemperatures in pelitic-psammitic metasedimentary rock samples from the Triassic-Lower Jurassic series displaying a clear mylonitic fabric. The selected samples have been also used to measure calcite CPO as reported in the previous section.

[19] Raman analyses were performed using a Renishaw (Wotton-under-Edge, UK) InVIA Reflex microspectrometer (ENS Paris). Before each session, this spectrometer was calibrated with silicon standard. The light source is a 514 nm Spectra Physics argon laser. The output laser power is around 20 mW but only around 1 mW reached the surface sample through DMLM Leica (Wetzlar, Germany) microscope with a 100× objective (NA = 0.90). Edge filters eliminated the Rayleigh diffusion, and the Raman light was then dispersed using 1800 g mm^{-1} grating before being analyzed by a Peltier cooled RENCAM CCD detector. Measurements have been done on polished thin sections cut normal to the foliation and parallel to the lineation (*XZ* structural plane).

To avoid the effect of polishing, the CM analyzed were below a transparent adjacent mineral, usually quartz or calcite. The scanning mode was extended from 1000 to 2000 cm^{-1}, and the acquisition time was typically between 10 and 60 s. To check the within-sample structural heterogeneity, more than 10 analyses were performed on each sample. Spectra were then decomposed using Voigt profile for all bands and the Peakfit software [*Beyssac et al*., 2003].

[20] The results obtained for the six analyzed samples are presented in Table 1. For five samples, the estimated temperatures range between 337°C and 387°C. For one sample (10AG4B) of Triassic limestones from an anhydrite-rich layer, a temperature of 494°C was obtained, contrasting significantly with the temperature of 387°C obtained for a sample (10AG4) located about 10 m above. This result requires further confirmation since it lies significantly out of the temperature range obtained for the five other samples. It is, however, worth remarking that the sampled layer rests about 1 m above the contact with Paleozoic schists.

[21] These temperature estimates are in good agreement with those obtained by *Goldberg and Leyreloup* [1990] in the sedimentary cover north of the Agly basement massif. The limited number of analyses does not allow extrapolating these temperatures at the scale of the Agly massif since it was shown that the Mesozoic metamorphism was influenced by seawater percolation in the crust [*Goldberg and Leyreloup*, 1990]. However, the homogeneity of the mylonitic structure over a large area requires a synkinematic temperature high enough to activate dislocation creep in calcite, i.e., in the range of the temperature estimates obtained in this study.

6. Discussion and Conclusions

[22] New field observations, crystallographic measurements, and temperature estimates collectively support that, during the Late Cretaceous, the Mesozoic cover that borders the Agly basement massif to the North was involved in a medium temperature, low-angle ductile shear zone localized at the boundary between the two formations. This mylonitic deformation accommodated a décollement, at least partial, of the sedimentary cover from the top of the Paleozoic basement. At the regional scale, this décollement is well documented by the basal truncation of the Mesozoic sedimentary sequence, which was already stressed by *Durand-Delga* [1964] and well described by *Berger et al*. [1993] on the 1:50.000 geological map of Rivesaltes (especially close to the towns of Estagel and Baixas). Refolding of the foliation and lineation associated to this shear zone by EW-trending Pyrenean (Eocene-Oligocene) folds supports that the formation of this ductile fabric predates the "Pyrenean" compression. Crystallization of scapolite crystals parallel to the lineation, deformation of limestones through crystal plasticity, and temperature estimates similar to those obtained for the Late Cretaceous metamorphism described in this area [*Goldberg and Leyreloup*, 1990] consistently support that ductile shearing was coeval with this preorogenic metamorphism and, consequently, with the Aptian-Albian formation of the Boucheville basin.

Table 1. Paleotemperatures Estimated Using the R^2 Raman Parameter From *Beyssac et al*. [2002] for Six Mylonitic Limestones[a]

Sample	Nb Spectra	R^2	SD	T (°C)	SE (°C)
10AG1B	15	0.64	0.01	356	2
10AG2B	14	0.68	0.03	337	4
10AG3	14	0.65	0.02	351	3
10AG4	12	0.57	0.05	387	6
10AG4B	13	0.33	0.06	494	7
10AG6	13	0.67	0.02	342	10

[a] R^2 is the ratio of the peak areas of the defect bands measured in the CM Raman spectra. SD is standard deviation; SE is standard error.

[23] The mylonites bear a N- to NE-trending mineral stretching lineation and display top-to-north (or NE) macroscopic and microscopic shear criteria, suggesting a "normal fault" kinematics. This kinematics is supported by the lack of lithological inversion and by the discontinuity of Triassic and lowermost Jurassic sediments (see cross section on Figure 2). However, chocolate tablet boudinage and paucity of kinematic indicators suggest a pure shear component normal to the foliation, likely due to loading by the sedimentary pile above the ductile shear zone. The kinematics is in agreement with an extensional deformation localized in the lower part of the Mesozoic pile resulting in the exhumation of the Agly basement massif. Strain localization at the boundary between Paleozoic and Mesozoic formations was probably favored by the low-viscosity evaporite layers within the Triassic sediments that were heavily boudinaged and only subsists as lenses of various sizes along the contact. The mylonitic microstructure of Triassic and Jurassic limestones, characterized by a very fine grain size, suggests relatively high-stress conditions. Considering the temperature conditions estimated in this study (340–390°C) and the lack of evidence of annealing, high deviatoric stress conditions might result from a rather high strain rate [*de Bresser et al*., 1993] and thus a rather fast exhumation of the Agly massif.

6.1. Microstructure, CPO, and Deformation Mechanisms

[24] Several samples display a concentration of calcite ***c***[0001] close to the pole to the foliation and a dispersion of $\boldsymbol{a}<2\bar{1}\bar{1}0>$ in the foliation plane. This pattern, which is interpreted as due to dislocation creep with (0001) as dominant slip plane, is rather frequent in calcite mylonites deformed under medium/high temperature conditions [e.g., *de Bresser and Spiers*, 1993; *Austin et al*., 2008]. The dispersion of $\boldsymbol{a}<2\bar{1}\bar{1}0>$ in the foliation plane may be due to a deformation regime involving a pure shear component orthogonal to the foliation. *Austin et al*. [2008] have recently shown that this slip system is dominant in calcite mylonites forming the sole of the Morcles nappe and that the CPO maintains the same pattern and tends to become stronger approaching the basal contact of the nappe. This evolution contrasts with the evolution of the CPO observed in the North Agly extensional shear zone where the concentration of ***c***[0001] close to the foliation pole tends to fade in samples with the finest grain size. In these samples, ***c***[0001] close to the foliation pole are only maintained for the coarser-grained fraction, whereas in the finest-grained size fraction ***c***[0001] tend to preferentially concentrate close to the lineation. The contrast between the CPO evolution in the Morcles Nappe and the North Agly extensional shear zone suggests that different deformation mechanisms have operated during the deformation of limestones in these two mylonitic zones. Although understanding such contrast requires further studies, it might be an effect of the strain regime: compressional in the Morcles nappe and extensional in the North Agly décollement zone.

[25] In the North Agly extensional shear zone, the small recrystallized grain size, the weak CPOs, and the variation of the CPO with the grain size in rocks displaying evidence of rather large deformation suggest that dislocation creep is not the only strain-accommodating mechanism. An additional, grain size–sensitive creep mechanism that weakens the crystallographic preferred orientation should significantly contribute to strain accommodation. However, the variation in calcite CPO between very small recrystallized "new" grains and the remaining parent grains in some mylonitic samples suggest that this additional mechanism generates a weak but well-defined preferred orientation of calcite new grains. Grain boundary sliding (GBS) is frequently invoked as strain-accommodating mechanism in very fine-grained aggregates. However, GBS by itself does not generate CPO nor elongate grain shapes. Two types of GBS with different plastic accommodation mechanisms are described in the literature [*Baudelet et al.*, 1975; *Langdon*, 1994, 2000, 2006]: (1) dislocation creep-assisted GBS [*Rachinger*, 1952; *Mukherjee*, 1971] and (2) diffusion creep-assisted GBS [*Lifshitz*, 1963; *Langdon*, 2000]. The grain shape in the aggregate deforming through GBS is equidimensional when the accommodation mechanism is dislocation creep, while grains display an elongation when diffusion creep is the accommodation mechanism [e.g., *Langdon*, 2006]. In the studied mylonitic limestones, the recrystallized grains of calcite, even the smallest, usually display a slightly elongate shape (up to 3:1). This observation does not fit well the expected equidimensional shape for dislocation creep-assisted GBS; it rather favors diffusion creep–assisted GBS. This mechanism might have been enhanced by the presence of fluids during deformation (as suggested by calcite fringes around quartz grains). It might also explain the unusual CPOs of calcite characterized by ***c***[0001] preferentially oriented parallel to the lineation (i.e., the extension direction), which characterizes the very fine-grained aggregates. It is noteworthy that such calcite CPO was not observed in coarser-grained aggregates or in parent grains.

6.2. Preorogenic Exhumation Model

[26] A ductile, extensional shear-zone coeval with the mid-Cretaceous metamorphism developed on the northern flank of the Agly basement massif. During the same period of time, a large basin (the Boucheville basin) developed South of the Agly massif in relation with the displacement of Iberia relative to Europa. This suggests that, during the Upper Cretaceous, extension affected not only a corridor along which Iberia moved but also the margin of Europa, resulting in a thinning of the continental Eurasian lithosphere. The consistent N- to NE-trending lineations observed in the Measozoic limestone north of the Agly basement massif are not in agreement with the deformation expected in pull-apart basins formed along the North Pyrenean Fault. More data, especially from other North Pyrenean basement massif are necessary to reliably decide which plate tectonic model is best. However, the new data from the Agly massif suggest that the Late Cretaceous extension affected a large domain of the Eurasian margin, and this does not fit well the "pull-apart basins" model.

[27] The extended middle to lower crust (the basement massifs, bounded by extensional domains) was tilted along the fault bounding the Boucheville basin to the North as suggested by the occurrence of the deepest metamorphic rocks close to the boundary with the Late Cretaceous basin. Tilting to the North likely favored the exhumation of the basement massif since it made the décollement of the Mesozoic cover on its northern side easier. Temperature increase and possible fluid transfer through the crust due to lithospheric thinning allowed limestone to deform through crystal plasticity and diffusion. In addition, evidence that large extension occurred within the pre-Albian Mesozoic cover and accommodated basement exhumation suggests that major extensional, low-temperature shear zones observed within the Agly basement may be related to the Upper Cretaceous extension, as it is the case for the Saint Barthelemy extensional shear zone [*Passchier*, 1984, *Saint Blanquat*, 1990).

[28] Figure 13 shows a conceptual model that summarizes the observations made in and around the Agly massif. In this model, the main extension occurs south of the massif where a large and deep basin develops, and an extensional domain is induced north of the Agly massif. This resulted in an asymmetrical exhumation, with the southern limb being significantly more exhumed than the northern limb, resulting in a tilting of the Agly massif. The development of an extensional detachment zone on the northern flank of the Agly massif is consistent with the results of numerical modeling of metamorphic core complexes by *Tirel et al.* [2008]: in all

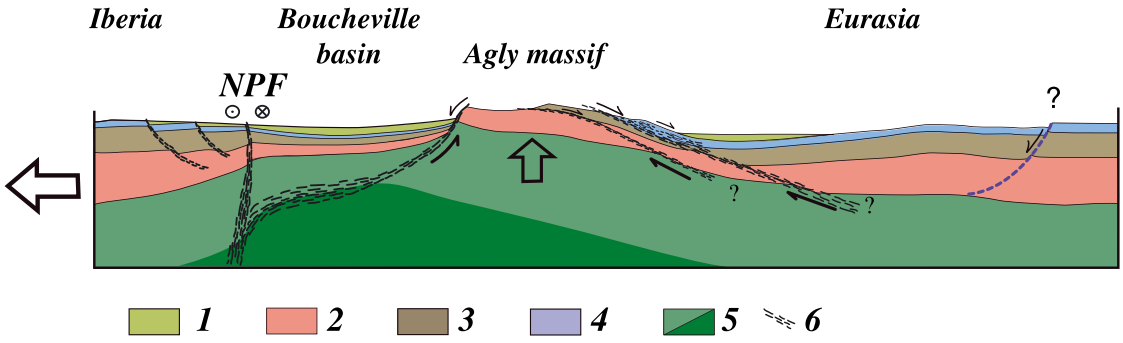

Figure 13. Cartoon showing a conceptual model for the exhumation of the Agly basement massif during the Late Cretaceous. The subsidence associated to the development of the Boucheville basin is compensated by the uplift, then the exhumation of the Agly massif through the development of an extensional shear at the boundary between the Mesozoic sequence and the basement. NPF represents the limit of the Iberian microplate, i.e., the future North Pyrenean Fault. 1 = subcontinental mantle, 2 = lower crust, 3 = Palaeozoic metasediments, 4 = Triassic to Aptian, 5 = Early Albian and 6 = faults/shear zones.

models with an initial Moho temperature (TMi) = 830°C, detachment zones developed on the dome limb opposite to the moving boundary. Even under higher temperature initial conditions (TMi = 1070°C), *Tirel et al*. [2008] models show that the main detachment zone develops on the dome limb opposite to the moving boundary for high boundary velocities and on the side of the moving boundary for low boundary velocities.

[29] The Agly massif appears as a key area to study the high-temperature deformation that affected the Mesozoic sediments and especially limestones of the North Pyrenean Zone during the detachment of Iberia from Europa. From this example, we suggest that the preorogenic exhumation process deduced from the observations in and around the Agly massif may account for the exhumation of the basement massifs exposed along the North Pyrenean belt. Strongly sheared metamorphic limestones, as those observed in the Agly massif, might represent a source for the HT mylonitic marble clasts that form thick breccia sequences observed in Albian basins, for instance, the Aulus basin [*Clerc et al*., 2012]. Considering that many North Pyrenean basement massifs, including the Agly massif, display lower crustal formations in tectonic contact with upper Cretaceous metasediments, the suggested widespread extensional deformation of the Southern Europa lithosphere may also have induced the exhumation of the mantle peridotites exposed along the belt, leading to their remobilization by sedimentary processes [*Lagabrielle and Bodinier*, 2008].

[30] **Acknowledgments.** The authors are indebted to Christophe Nevado and Doriane Delmas for preparing carefully polished thin sections and to Andrea Tommasi and Fabrice Barou for their help in the measurement of the crystallographic orientation of very fine grains. We acknowledge Anne Delplanque for assistance with the drawings.

References

Austin, N., B. Evans, M. Herwegh, and A. Ebert (2008), Strain localization in the Morcles nappe (Helvetic Alps, switzerland). *Swiss J. Geosci. 101*, 341–360.

Bachmann, F., R. Hielscher and H. Schaeben (2010), Texture analysis with MTEX—free and open source software toolbox. *Solid State Phenom. 160*, 63–68.

Baudelet, B., M. Suery, and A. Eberhardt (1975). Le glissement aux joints et les mécanismes accommodateurs. *J. Phys. 36*, 281–289.

Berger, G. M., Fonteilles A. F., Leblanc D., Clauzon G., Marchal C., Vautrelle C. (1993), Notice explicative, carte géologique de la France (l/50.000). *feuille Rivesaltes, BRGM*, 194 p.

Beyssac, O., B. Goffé, C. Chopin and J. N. Rouzaud (2002), Raman spectra of carbonaceous material in metasediments: A new geothermometer. *J. Metamorph. Geol. 20*, 859–871.

Beyssac, O., B. Goffé, J.-P. Petitet, E. Froigneux, M. Moreau and J.-N. Rouzaud (2003), On the characterization of disordered and heterogeneous carbonaceous materials by Raman spectroscopy. *Spectrochim. Acta A Mol. Biomol. Spectrosc. 59*, 2267–2276.

Bouhallier, H., P. Choukroune and M. Ballèvre (1991), Evolution structurale de la croûte profonde Hercynienne: Exemple du massif de l'Agly (Pyrénées orientales, France). *Comptes Rendus Acad. Sci. II 312*, 647–654.

Choukroune, P. (1992), Tectonic evolution of the Pyrenees. *Annu. Rev. Earth Planet. Sci.*, *20*, 143–158.

Choukroune, P. and M. Mattauer (1978), Tectonique des plaques et Pyrenées: Sur le fonctionnement de la faille transformante nord-pyrénéenne; comparaison avec les modèles actuels. *Bull. Soc. Géol. France 20*, 689–700.

Clerc, C., Y. Lagabrielle, M. Neumaier, J.-Y. Reynaud and M. de Saint-Blanquat (2012), Exhumation of subcontinental mantle rocks: Evidence from ultramafic-bearing clastic deposits nearby the Lherz peridotite body, French Pyrenees. *Bull. Soc. Géol. France 183*, 443–459.

Costa, S. and H. Maluski (1988), Use of the 40Ar-39Ar stepwise heating method for dating mylonitic zones: An example from the St. Barthélémy Massif (Northern Pyrenees, France). *Chem. Geol. 72*, 127–144.

de Bresser, J. H. P. and C. J. Spiers (1993), Slip systems in calcite single crystals deformed at 300–800°C. *J. Geophys. Res. 98*, 6397–6409.

de Bresser, J. H. P., B. Evans, and J. Renner (2002), On estimating the strength of calcite rocks under natural conditions. *Geol. Soc. London Spec. Publ. 200*, 309–329.

Durand-Delga, M. (1964), Remarques sur la stratigraphie et la structure du Mésozoïque situé entre Estagel et Perpignan (Pyrénées-Orientales), *Comptes Rendus de l'Académie des Sciences de Paris*, *259*, 837–840.

Goldberg, J. M. and A. F. Leyreloup (1990), High temperature–low pressure Cretaceous metamorphism related to crustal thinning (Eastern North Pyrenean Zone, France). *Contrib. Mineral. Petrol. 104*, 194–207.

Hielscher, R. and H. Schaeben (2008), A novel pole figure inversion method: Specification of the MTEX algorithm, *J. Appl. Cryst. 41*, 1024–1037.

Lagabrielle, Y. and J.-L. Bodinier (2008), Submarine reworking of exhumed subcontinental mantle rocks: Field evidence from the Lherz peridotites, French Pyrenees. *Terra Nova 20*, 11–21.

Lagabrielle, Y., P. Labaume and M. de Saint Blanquat (2010), Mantle exhumation, crustal denudation, and gravity tectonics during Cretaceous rifting in the Pyrenean realm (SW Europe): Insights from the geological setting of the lherzolite bodies. *Tectonics 29*, TC4012.

Langdon, T. G. (1994), A unified approach to grain boundary sliding in creep and superplasticity. *Acta Metall. Mater. 42*, 2437–2443.

Langdon, T. G. (2000), Identifiying creep mechanisms at low stresses. *Mater. Sci. Eng. A283*, 266–273.

Langdon, T. G. (2006), Grain boundary sliding revisited: Developments in sliding over four decades. *J. Mater. Sci. 41*, 597–609.

Larrasoaña, J. C., J. M. Parés, J. del Valle, and H. Millán (2003), Triassic paleomagnetism from the Western Pyrenees revisited: Implications for the Iberian-Eurasian Mesozoic plate boundary, *Tectonophysics 362*, 161–182.

Legier, C., C. Tempier, A. Vauchez (1987), Tectonique tangentielle ductile syn-metamorphe d'age Cretace superieur dans la couverture du massif de l'Agly (zone nord-pyreneenne orientale). *Comptes Rendus Acad. Sci. II 305*, 907–911.

Le Pichon, X., J. Bonnin, and J.-C. Sibuet (1970), La faille nord-pyrénéenne: Faille transformante liée à l'ouverture du Golfe de Gascogne, *Comptes Rendus Acad. Sci. II*, *271*, 1941–1944.

Lifshitz, I. M. (1963), On the theory of diffusion-viscous flow of polycrystalline bodies. *Soviet Phys.-J. Exp. Theor. Phys. Lett. 17*, 909–920.

Mainprice, D., R. Hielscher, H. Schaeben (2011), Calculating anisotropic physical properties from texture data using the MTEX open-source package. *Geol. Soc. London Spec. Publ. 360*, 175–192.

Mukherjee, A. K. (1971), The rate controlling mechanism in superplasticity. *Mater. Sci. Eng. 8*, 83–89.

Paquet, J. and J.-L. Mansy (1991), La structure de l'Est des Pyrénées (transversales du massif de l'Agly): Un exemple d'amincissement crustal. *Comptes Rendus Acad. Sci. II 312*, 913–919.

Passchier, C.W. (1984), Mylonite dominated footwall geometry in a shear zone, central Pyrénées, *Geol. Mag.*, *121*, 429–436.

Pieri, M., K. Kunze, L. Burlini, I. Stretton, D. L. Olgaard, J. P. Burg, and H. R. Wenk (2001), Texture development of calcite by deformation and dynamic recrystallization at 1000°K during torsion experiments of marble to large strains, *Tectonophysics 330*, 119–140.

Poujol, M., P. Boulvais and J. Kosler (2010), Regional-scale Cretaceous albitization in the Pyrenees: Evidence from in situ U-Th-Pb dating of monazite, titanite and zircon. *J. Geol. Soc. 167*, 751–767.

Rachinger, W. A. (1952), Relative grain translations in the plastic flow of aluminium. *J. Inst. Met. 81*, 33–41.

Saint-Blanquat, M., Bunel, M. and Mattauer, M., (1986), Les zones de cisaillement du massif Nord-pyrénéen du Saint-Barthélémy témoins probables de l'extension crustale d'âge crétacé. *Comptes rendus de l'Académie des sciences, Série 2*, *303*, 1339–1344.

Saint Blanquat, M. (1990), Petrological argument for high temperature extensional deformation in the Pyrenean Variscan crust (Saint Barthélémy Massif, Ariège, France). *Tectonophysics 177*, 245–262.

Saint Blanquat, M., (1993), La faille normale ductile du massif du Saint Barthélémy. Evolution hercynienne des massifs nord-pyrénéens catazonaux considérée du point de vue de leur histoire thermique, *Geodinamica Acta*, *6*, 59–77.

Schärer, U., P. de Parseval, M. Polvé and M. de Saint Blanquat (1999), Formation of the Trimouns talc-chlorite deposit (Pyrenees) from persistent hydrothermal activity between 112 and 97 Ma. *Terra Nova 11*, 30–37.

Sibuet, J.-C., S. P. Srivastava, and W. Spakman (2004), Pyrenean orogeny and plate kinematics, *J. Geophys. Res. 109*(B08104).

Srivastava, S. P., H. Schouten, W. R. Roest, K. D. Klitgord, L. C. Kovacs, J. Verhoef, and R. Macnab (1990), Iberian plate kinematics: A jumping plate boundary between Eurasia and Africa, *Nature 344*, 756–759.

Stampfli, G. r. M., and C. Hochard (2009), Plate tectonics of the Alpine realm, *Geol. Soc. London Spec. Publ. 327*, 89–111.

Tirel, C., J.-P. Brun and E. Burov (2008), Dynamics and structural development of metamorphic core complexes. *J. Geophys. Res. 113*, B04403.

Vielzeuf, D. and J. Kornprobst (1984). Crustal splitting and the emplacement of the Pyrenean lherzolites and granulites. *Earth Planet. Sci. Lett.*, *67*, 87–96.

Wopenka, B. and J. D. Pasteris (1993), Structural characterization of kerogens to granulite-facies graphite; applicability of Raman microprobe spectroscopy. *Am. Mineral. 78*, 533–557.